A MATHEMATICAL MODEL FOR COMBINING DATA FROM A TELESCOPE WITH THE INFORMATION ABOUT THE ORBITAL DEBRIS ENVIRONMENT THAT IS CONTAINED IN TWO LINE ELEMENT SET FILES

T.J. Hebert[1,2], E.G. Stansbery[3]

[1] *Dept. of Electrical and Computer Engineering, Univ. of Houston, 77204-4793 USA, thebert@uh.edu*
[2] *Liberated Technical, Houston, TX 77058*
[3] *NASA Johnson Space Center, Houston, TX, USA, eugene.g.stansbery1@ jsc.nasa.gov*

ABSTRACT

This paper presents an optimal framework for combining information contained in two line element (TLE) files with sensor measurement data to estimate the orbital debris environment. This method can be applied to radar as well as optical data. Results from applying this method to data from the NASA liquid mirror telescope demonstrate an improvement in accuracy and a marked reduction in uncertainty in estimates of the orbital debris environment.

1. INTRODUCTION

Our most detailed (though incomplete) insight into the orbital debris environment is provided by the United States Space Surveillance Network (SSN). The SSN tracks and maintains the orbital elements and radar cross sections (RCS) of close to nine thousand objects (ten thousand objects if temporary numbers in the eighty thousand range are included). This information is provided in two-line element (TLE) set files and SSN catalog files. Ideally, one would like these files to contain a complete list of all objects of a given limiting size and larger in orbit, but this is not possible. Therefore, to characterize the orbital debris environment in a statistical sense, the Orbital Debris Program Office at the NASA Johnson Space Center uses additional radar and optical sensors having little or no tracking capability. Flux measurements from these sensors represent a very different type of information from that of the SSN catalog and TLE files. Flux measurements relate to the entire unknown orbital population, while SSN catalog/TLE file information relates to a known "labeled" subset of objects. Catalog/TLE files contain complete/accurate measurements of the orbital parameters of "labeled" objects in orbit, while flux measurements contain incomplete/less-accurate information about the orbital parameters of an "anonymous" subset of objects that by chance crossed the field of view of the non-tracking radar or telescope. The orbital parameters of this "anonymous" subset of objects are then used to infer the orbital debris environment in a statistical sense.

Consider the case where a telescope/radar detects an object for which the orbital parameters and radar cross section (RCS) are available from the SSN. The accuracy of the orbital elements that can be inferred from a single observation (optical/radar) of that object is less than the accuracy in the TLE file that is based on many observations of the object. Similarly, the accuracy of the object's size inferred from a single observation (optical/radar) is less than that which can be inferred from the SSN history of RCS measurements. Therefore, if a telescope/radar detects an object whose orbital parameters and RCS are maintained by SSN, the optical/radar detection of that object represents essentially no new information about the debris environment.

A statistical characterization of the orbital debris environment would be improved by incorporating the high precision, "labeled" information is the SSN TLE/RCS files. This paper presents an optimal mathematical framework for combining the statistical information about the orbital environment contained in flux measurements with the deterministic information contained in SSN TLE/RCS files.

2. MATHEMATICAL METHOD FOR COMBINING MEASUREMENT DATA WITH SSN TLE/RCS FILES

Consider the distinction between the measurement of flux as recorded by a sensor and the use of those measurements to estimate the true flux in the orbital environment. For example, consider a 0.1 m telescope with a 0.6 degree FOV placed next to a 1.0 m telescope with a 0.3 degree FOV. Both telescopes view essentially the same orbital flux but record different measurements of that flux. The wider FOV allows the 0.1 m telescope to acquire a better sample of the population of large objects in orbit, *i.e.* one whose variance is less than that of the 1.0 m telescope. Similarly, the 1.0 m telescope's better detection sensitivity for smaller objects allows it to acquire a better sample of the small objects in orbit. The measurement of same orbital flux from these two sensors will yield different values. This goes beyond sensor sensitivity when one also considers differences in

Proceedings of the 3rd European Conference on Space Debris, ESOC, Darmstadt, Germany, 19 - 21 March 2001
(ESA SP-473, August 2001)

noise/error factors in the two measurement sets. One factor is that meteors arriving from radiant directions near the direction of the FOV can appear identical to a piece of orbital debris crossing the FOV. The random detection of meteors that appear to be debris will also be different for the two telescopes. Thus there is a difference between listing the flux measurement itself as opposed to estimating the orbital flux by correcting those measurements for detection sensitivity, noise/error factors, as well as the relative uncertainty in each aspect of the measurement (size, inclination, altitude, etc.).

Consider the maximum likelihood formulation [1] for estimating the mean orbital flux based on both the detected objects (orbital parameters, sizes) and the information in the SSN TLE/RCS files. Let the measurements (orbital parameters, sizes) associated with all detected objects be contained in an ordered vector $\vec{\mathbf{d}}$. Let the SSN information (orbital parameters and history of RCS measurements) from all tracked objects be contained in an ordered vector $\overrightarrow{\mathbf{ssn}}$. Similarly, the unknown mean orbital flux at all (altitude, inclination) pairs be denoted by ordered vector $\vec{\mathbf{f}}$. Vector $\vec{\mathbf{f}}$ is to be statistically inferred from vector $\vec{\mathbf{d}}$ (ground-based sensor measurements having limited sensitivity as well as measurement error) and vector $\overrightarrow{\mathbf{ssn}}$ (highly accurate measurement information on a limited set of objects). Measurements $\vec{\mathbf{d}}$ and $\overrightarrow{\mathbf{ssn}}$ are conditionally independent and represented a random number of observed objects and their associated measurements. Maximum likelihood estimation of flux $\vec{\mathbf{f}}$ requires solution of the problem

$$\max_{\vec{\mathbf{f}}} \; \mathrm{p}\left(\vec{\mathbf{d}}, \overrightarrow{\mathbf{ssn}} \,|\, \vec{\mathbf{f}}\right) \quad . \tag{1}$$

Conceptually, one can divide the set of all objects in orbit into two mutually exclusive sets: the set of all tracked CT objects found in the TLE files and the set of all non-tracked UCTs in the environment. Since these two sets are mutually exclusive, the flux in the environment is the superposition of the fluxes (sum of responses) from these two sets. Therefore, orbital flux above a sensor is separable into that from SSN objects $\vec{\mathbf{f}}^{\,\mathrm{c}}$ and that from uncorrelated objects $\vec{\mathbf{f}}^{\,\mathrm{u}}$

$$\vec{\mathbf{f}} = \vec{\mathbf{f}}^{\,\mathrm{c}} + \vec{\mathbf{f}}^{\,\mathrm{u}} \, . \tag{2}$$

In addition, objects detected in the sensor measurements and their measured orbital parameters can be similarly assigned to either the set of measured CT objects $\vec{\mathbf{d}}^{\,\mathrm{c}}$ or the set of measured UCT objects $\vec{\mathbf{d}}^{\,\mathrm{u}}$. This is done by correlating the detected objects with objects in the SSN TLE file (the TLE file nearest the date of each measurement data set) so that

$$\{\vec{\mathbf{d}}\} = \{\vec{\mathbf{d}}^{\,\mathrm{c}}, \vec{\mathbf{d}}^{\,\mathrm{u}} \,|\, \overrightarrow{\mathbf{ssn}}\} \, . \tag{3}$$

For objects in non-specialized orbits, a theoretical mean cross sectional flux from a single object in a single TLE file can be computed by uniformly distributing the object's argument of perigee and ascending node over 2π [3]. Where α denotes altitude for $\alpha_{\mathrm{peri}} < \alpha < \alpha_{\mathrm{apog}}$, β denotes declination, μ is the gravitational parameter, $R_{\oplus}$ denotes mean equatorial radius, a is the semi-major axis, and i is orbital inclination of the object, the mean cross-sectional flux at a single point is well-modeled as [3]

$$\mathrm{flux}_{\mathrm{CS}}(\alpha,\beta) = \frac{\sqrt{\dfrac{2\mu}{\mathrm{R}_{\oplus}+\alpha} - \dfrac{\mu}{a}}}{a 2\pi^3 \left[\mathrm{R}_{\oplus}+\alpha\right]\sqrt{\chi}} \tag{4}$$

where $\chi = \left[\sin^2(i) - \sin^2(\beta)\right]\left[\alpha - \alpha_{\mathrm{peri}}\right]\left[\alpha_{\mathrm{apog}} - \alpha\right]$

where $\mathrm{flux}_{\mathrm{CS}}(\alpha,\beta)$ is in units of number per $(\mathrm{km}^2 \cdot \mathrm{sec})$. The set of objects in non-specialized orbits includes debris from satellites in specialized orbits. Objects in specialized orbits, particularly sun-synchronous objects, can be handled separately but in similar fashion.

Using the SSN TLE/RCS information $\overrightarrow{\mathbf{ssn}}$, the theoretical mean CT flux $\vec{\mathbf{f}}^{\,\mathrm{c}}$ from all TLE objects can thus be computed

$$\vec{\mathbf{f}}^{\,\mathrm{c}} = \vec{\boldsymbol{\phi}}\left(\overrightarrow{\mathbf{ssn}}\right) \tag{5}$$

Combining Eqs. (1),(2),(3) and (5)

$$\mathrm{p}\left(\vec{\mathbf{d}}, \overrightarrow{\mathbf{ssn}} \,|\, \vec{\mathbf{f}}\right) = \mathrm{p}\left(\vec{\mathbf{d}}^{\,\mathrm{c}}, \vec{\boldsymbol{\phi}}(\overrightarrow{\mathbf{ssn}}) \,|\, \vec{\mathbf{f}}^{\,\mathrm{c}}\right) \mathrm{p}\left(\vec{\mathbf{d}}^{\,\mathrm{u}} \,|\, \vec{\mathbf{f}}^{\,\mathrm{u}}\right) \quad . \tag{6}$$

Where measurement data is collected over many days, one need only be careful to use the time-average theoretical mean CT flux computed with the set of TLE files corresponding to the data collection times. Noting that $\vec{\mathbf{d}}^{\,\mathrm{c}}$ is redundant information, Eq. (2) reduces to

$$\max_{\vec{\mathbf{f}}^{\,\mathrm{c}}, \vec{\mathbf{f}}^{\,\mathrm{u}}} \left[\mathrm{p}\left(\vec{\mathbf{d}}^{\,\mathrm{u}} \,|\, \vec{\mathbf{f}}^{\,\mathrm{u}}\right) \delta\left(\vec{\boldsymbol{\phi}}(\overrightarrow{\mathbf{ssn}}) - \vec{\mathbf{f}}^{\,\mathrm{c}}\right)\right] \tag{7}$$

where $\delta(\cdot)$ is the dirac delta function. Since Eq. (7) holds for all $\mathrm{p}\left(\vec{\mathbf{d}}^{\,\mathrm{u}} \,|\, \vec{\mathbf{f}}^{\,\mathrm{u}}\right)$, the use of deterministic

methods for computing $\vec{\mathbf{f}}^{\,u}$ from $\vec{\mathbf{d}}^{\,u}$ is also supported in this approach.

Given the insight developed above, one may now correctly conclude that the detection of a CT object by a non-tracking sensor gives us no new information about the orbital debris environment. That is, we already know a CT object's orbital parameters and size with less uncertainty than is available from the non-tracking sensor. However, in the general sense, every datum contains information. Here, the detection of a CT object by a non-tracking sensor contains information, not about the environment, but about the sensor characteristics. The sensor characteristics are central to the use of that sensor to form a statistical description of the orbital debris environment. Therefore, we use the set of all CT detections by the sensor to calibrate the sensor for inference of the UCT portion of the orbital environment. To be more precise, form an estimate of mean CT flux from the sensor CT detections and form an estimate of mean UCT flux from sensor UCT detections. Compare the estimate of CT flux with the theoretical mean CT flux. The agreement or lack thereof between the estimate and the computed average flux indicates whether or not the UCT flux estimates are correctly calibrated. Given an acceptable calibration, form an estimate of the orbital environment as a superposition of the theoretical mean CT flux based upon SSN TLE/RCS files with the estimate of the mean UCT flux based upon UCT detections by the sensor.

The general method for combining measurement data with SSN TLE/RCS information is one that can be applied to radar or optical data. Fig. 1 shows a flow chart for the presented method. Note the inputs: (a) the detected objects, their estimated altitudes, inclinations, sizes, etc. and the universal times at which they were nearest the center of the FOV of the sensor; (b) TLE and RCS files for the dates nearest those during which the telescope data was collected. The outputs from this approach are: (a) calibration error - the difference between the theoretical flux from TLE objects and the measured CT flux. (b) an estimate of the orbital flux as a function of the parameters of interest.

The method begins by determining which objects detected by the sensor also appear in the TLE files. This is done by correlating their (space-time position, inclination, size) information with those from the TLE and RCS file. Detected objects found to be correlated (CTs) are moved to a separate data set that is then used to calibrate the detection sensitivity of the instrument. The remaining detected objects (UCTs) belong to the set of un-tracked objects and are used to estimate UCT orbital flux. The other component of orbital flux is that computed as the time-average theoretical mean flux from all objects in the TLE files used in the TLE correlation step. This mean CT flux is then added to the UCT flux to form the complete flux estimate.

3. APPLICATION TO NASA LMT DATA

NASA's liquid mirror telescope (LMT) located near Cloudcroft, New Mexico at latitude 32.98 N, longitude 105.73 W is a zenith-staring three-meter aperture 0.28-degree field of view (FOV) telescope. Digital videotapes recorded from the LMT are sent to the Johnson Space

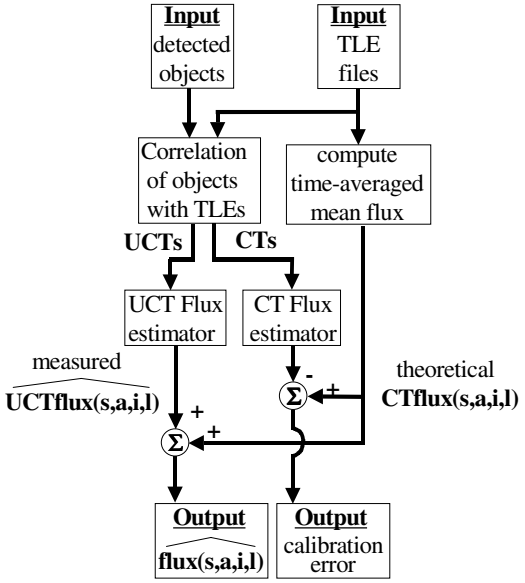

Fig. 1. Diagram of the measurement/TLE method for estimating mean flux.

Center (JSC), transferred onto PC, and processed with an automated detection software. Detected orbital debris, meteors, and satellites (to a maximum altitude of 64,000 km - assuming circular orbit) are reviewed using an operator controlled software that also performs photometric analysis of the object to determine its orbital parameters (assuming zero eccentricity) and size. A total of 160.2 hours of digital video data collected from March 1999 through June 2000 were processed by the automated detection software. The detected objects and their measurements were processed using the mathematical method for combining measurement data with SSN TLE/RCS information as described in section 2. Here, the goal was to estimate the time-average (March 1999-June 2000) mean orbital flux (above latitude 32.98 N) as a function of object size **s**, altitude **a**, inclination **i**, and an additional parameter **l** that establishes two separate sets of UCT objects - sun-synchronous (**l**=1) and non-sun-synchronous (**l**=0).

Using three TLE files from March 1999 to June 2000, a time-average theoretical flux $\vec{\phi}(\overrightarrow{ssn})$ from non-sun synchronous SSN TLE objects was computed. By correlating measurements $\vec{d}$ with objects in the SSN TLE file nearest the date at each measurement was acquired, a measurement set $\vec{d}^{\,c}$ for SSN TLE objects was constructed. All sun-synchronous objects were then removed from this set and each object's size was computed using a direct absolute magnitude-to-size mapping. A measured flux for non-sun synchronous SSN objects of size 10 cm or larger was then computed. Fig. 2 shows the ratio of measured flux to theoretical mean TLE flux as a function of altitude.

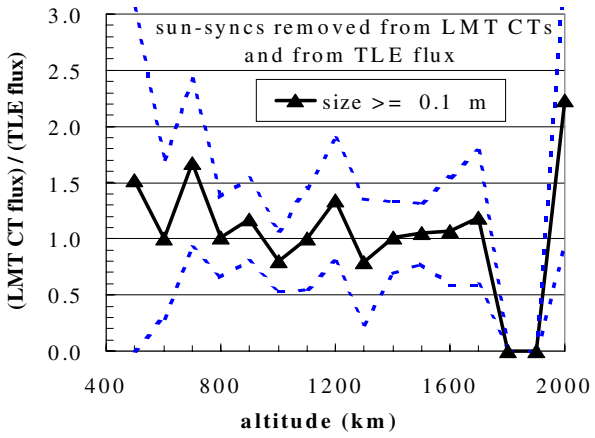

Fig. 2. The ratio of measured LMT flux from CT objects to theoretical mean TLE flux as a function of altitude. The dotted lines show the effect of plus or minus the square root of the number of detected SSN TLE objects at each altitude.

Given an infinite amount of observation time and a perfectly calibrated sensor that could measure the complete set of orbital parameters for each object, ideally this plot would show a constant value of 1.0 at all altitudes. This plot does shows reasonably good calibration of the LMTs observational capability. Note that no SSN objects were observed between 1750 km and 1950 km so that the ratio is 0.0. The dotted lines show the effect of plus or minus the square root of the number of detected SSN TLE objects at each altitude.

To compute an estimate of UCT flux $\vec{f}^{\,u}$ from measurements $\vec{d}^{\,u}$, it must be noted that for a narrow FOV telescope, meteors often appear visually indistinguishable from debris. This occurs more frequently for lower altitudes. Meteors emit light as they ablate in the atmosphere, typically below 130 km. Debris in orbit on the other hand can only be seen under meteors and debris is the comparison between the altitude of the earth's shadow at the time the object is observed and the measured altitude of the object. Therefore, before a detected object is labeled as debris (UCT), it must first be determined to be above the altitude of the earth's shadow at the time it is observed. However, some meteors are still present in $\vec{d}^{\,u}$ after this step. Meteors that appeared to be debris but were removed on the basis of shadow height at the time of detection can be used to estimate the false-debris rate; *i.e.* the rate versus altitude at which meteors that are indistinguishable from debris cross the LMT FOV. Fig. 3 shows the measured false-debris rate versus altitude for the 1999-2000 LMT data set.

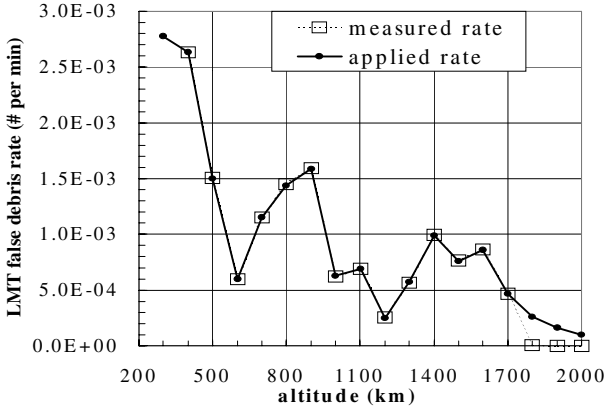

Fig. 3. Estimated rate versus altitude at which meteors that are indistinguishable from debris cross the LMT FOV.

Finally, since the LMT only takes observations during the two hours preceding dawn and two hours following dusk, there is an observational bias towards detecting sun synchronous objects with ascending nodes near the dawn or dusk points. Due to nodal drift, orbit maintenance is required to retain an object in sun-synchronous orbit. However, LMT objects $\vec{d}^{\,u}$ are not tracked by SSN and as such are anticipated to be debris objects that are not undergoing orbit maintenance. Nevertheless, nodal drift can take years to move an object out of an approximate sun synchronous orbit. The identification of sun-sync debris within $\vec{d}^{\,u}$ is done on the basis of altitude and inclination. The dominant secular motion caused by J_2, the relationship between semi-major axis *a*, eccentricity *e*, and inclination *i* can be formed [4]. Based on measured altitudes and inclinations, the criteria (a) measured altitudes may represent any altitude between perigee and apogee, (b) object eccentricities of 0.0 to 0.4, lead to the following range of inclinations *i* within which an object may be in sun-synchronous or near sun-synchronous orbit.

Applying these criteria, constraints on inclination *i* and altitude *alt* are derived from [4]. All objects satisfying those constraints were labeled as sun-sync objects with ascending nodes near the longitude of sunrise or sunset. According to these criteria, 11.9% of the UCT objects detected by the LMT in the 1999-2000 data set were such objects.

The LMT always observes during the two hours preceding sunrise or the two hours following sunset. This lends an observational bias towards detecting a disproportionately large number of sun-synchronous objects. This only applies to sun-sync objects with ascending nodes near the longitude of sunrise or sunset. Fig. 4 demonstrates this observational bias. The spatial density from a sun-synchronous or near sun-synchronous objects is always concentrated near the LMT FOV during its 2-hour observation periods. Conversely, the node of most objects precesses over 2π several times during the 12-18 months that comprise a single data set. For such a time span, the spatial density of each object is spread out over a region such as that shown in Fig. 4.

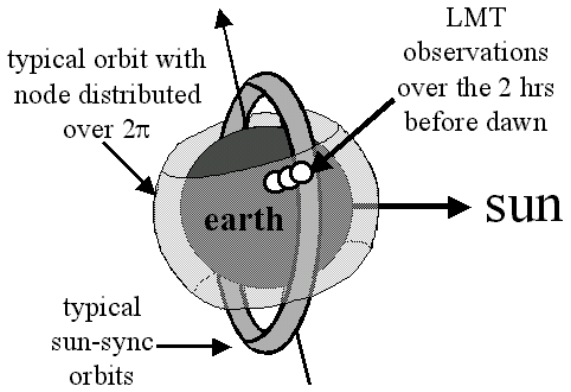

Fig. 4. Diagram showing the earth-sun vector, a region for typical sun-synchronous orbits, and a typical non-sun-synchronous orbital region with the node distributed over 2π.

To correct for observational bias towards detecting debris generated in sun-sync orbits with ascending nodes near the longitude of sunrise or sunset, we apply the following model. Consider the vector $\vec{\mathbf{v}}_{ed}^{k}(t)$ from earth-center to the k^{th} debris object generated in such a sun-sync orbit. We now apply two conditions: (a) Let $\vec{\mathbf{v}}_{es}(t)$ denote the vector from earth-center to sun-center and let $\theta_k(t)$ denote angle between $\vec{\mathbf{v}}_{ed}^{k}(t)$ and $\vec{\mathbf{v}}_{es}(t)$. For all time *t*, model the set $\{\theta_k(t)\}_{k=0,1,..}$ as being symmetrically distributed about 90 degrees and bounded by 65 and 115 degrees. (b) Since debris are not undergoing periodic burns to $\{\theta_k(t)\}_{k=0,1,..}$ have a reduced probability of being near 90 degrees, and assign $\int_{105}^{115} p(\theta)\,d\theta = 0.25$ rather than the value 0.2 that would be obtained under an assumption of a uniform distribution. Based upon (a), (b), and a log of the observation times, for the 1999-2000 LMT data set, the sun sync bias versus altitude is shown in Fig. 5.

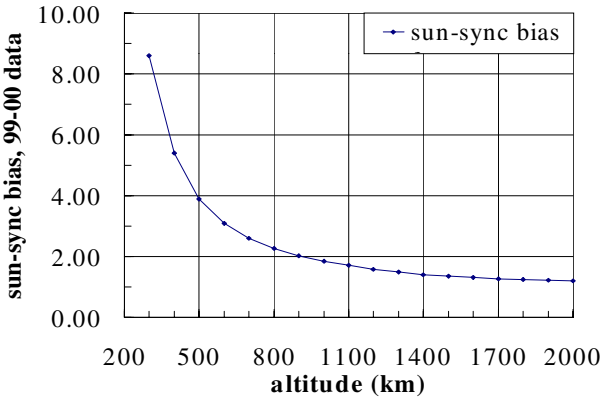

Fig. 5. Plot of the LMT bias factor versus altitude for the 1999-2000 LMT data set.

Consider two debris objects crossing an altitude of 800 km, only one of which is in sun-sync orbit. Under the applied model, the LMT is more than 2.2 times more likely to detect the sun-sync object during any 2-hour observation period preceding sunrise or following sunset. Due to shadow height, the LMT typically views the 800-km region for about one-third of the full observation period. During these minutes, the LMT is viewing space in which the spatial density of a sun-sync object at 800 km is concentrated.

Applying both the sun-sync bias correction in Fig. 5 and the false-debris correction in Fig. 3, a comparison can be made between the standard method of computing flux from the combined CT and UCT detections versus the new method that fully incorporates SSN TLE/catalog information. Fig. 6 shows a comparison of surface area flux from the viewpoint of the standard method on a log-log plot. A comparison of cumulative flux rather than of flux itself does mask the differences between the results from the two methods, particularly at smaller sizes. Differences in cumulative flux in Fig. 6 range from 14.3% at 12.5-cm to 2.4% at 5-cm.

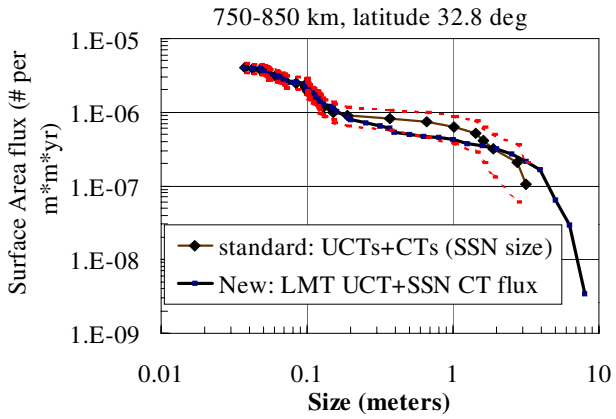

Fig. 6. Comparison of the standard method of computing flux by combining UCT and CT detections versus the new method of combining UCT detections with SSN TLE/catalog information.

Fig. 7 shows a comparison between LMT cumulative flux and radar flux from the Haystack radar [5]. Also shown in dotted lines are the LMT flux plus and minus the square root of the number of detected objects of a given size and larger.

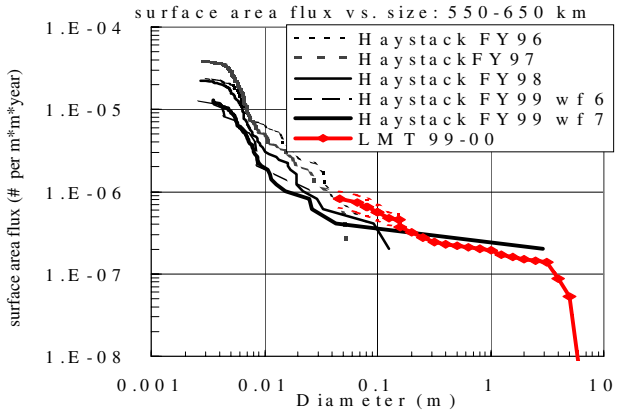

Fig. 7. Comparison of the LMT flux and Haystack flux.

4. CONCLUSIONS

The results from applying this method to data from the NASA liquid mirror telescope demonstrate an improvement in accuracy and a marked reduction in uncertainty in estimates of the orbital debris environment.

5. REFERENCES

1. Mendel J. (1995); Lessons in Estimation Theory for Signal Processing, Communications and Control, *Prentice Hall Signal Processing Series*, Englewood Cliffs, New Jersey.

2. Hebert T.J., Leahy R.M. (1992); Statistic-Based MAP Image Restoration from Poisson Data Using Gibbs Priors, *IEEE Trans on Signal Processing*, **40-9**, 2290-2303.

3. Kessler D.J. (1981), Derivation of the collision probability between orbiting objects: the lifetimes of Jupiter's outer moons, *ICARUS,* **48**, pp 39-48.

4. D.A. Vallado; Fundamental of Astrodynamics and Applications*; McGraw-Hill Space Technology Series,* 1997.

5. Settecerri T.J., Stansbery E.G., Hebert T.J. (1999); Radar Observations of the Orbital debris Environment: Haystack and Hax Radars Oct 1990-Oct 1998*, JSC-28744.*